Vol. 40, No. 2, November 2025, pp. 580~589

ISSN: 2502-4752, DOI: 10.11591/ijeecs.v40.i2.pp580-589

Detection of short circuit faults in two-level voltage source inverter using convolution neural network

Sai Aioub, Belghiti Zakariya, El Menzhi Lamiaâ

Departement of Electrical and Industrial Engineering, National School of Applied Sciences, Abdelmalek Essaadi University, Tangier, Morocco

Article Info

Article history:

Received Sep 9, 2024 Revised Jul 28, 2025 Accepted Oct 14, 2025

Keywords:

Diagnosis
Fault diagnosis
Lissajous curve
Machine learning
Voltage source inverter

ABSTRACT

Voltage source inverters (VSIs) play a critical role in modern industrial systems, particularly in controlling the operation of equipment such as induction motors. Ensuring their reliable performance is crucial, as faults like short circuits can severely disrupt industrial processes. This paper introduces a new diagnostic approach for detecting and localizing short circuit faults in VSIs. The method uses Lissajous curves derived from the Clark transformation of the VSI's 3-phase voltage components (V_{α}, V_{β}) . These curves serve as input data for a convolutional neural networks (CNNs) model, enabling the accurate classification of single and double short circuit faults. Simulation results using MATLAB/Simulink demonstrate that the proposed method achieves 100% classification accuracy within 100 ms, highlighting its suitability for real-time applications. The approach offers significant advantages in speed and accuracy over traditional techniques, with potential implications for enhancing the reliability and safety of inverter-driven systems in industrial environments.

This is an open access article under the CC BY-SA license.



580

Corresponding Author:

Sai Aioub

Departement of Electrical and Industrial Engineering National School of Applied Sciences, Abdelmalek Essaâdi University

Tangier, Morocco

Email: aioub.sai@etu.uae.ac.ma

1. INTRODUCTION

Voltage source inverters (VSIs) are vital components in power electronic systems, converting DC power to AC for applications ranging from industrial motor drives to renewable energy systems and electric vehicles. The widespread deployment of two-level VSIs stems from their simplicity and cost-efficiency. However, their power-switching semiconductors, particularly IGBTs, are susceptible to short-circuit faults, which can cause equipment failure, system shutdown, or severe damage if left undetected.

Over the past two decades, diverse fault detection methods have been proposed. These methods can be classified into: i) traditional signal-based approaches, ii) transform-based analysis methods, iii) AI-based detection methods, iv) hybrid combinations, and v) hardware-accelerated approaches, each with unique advantages and limitations.

Traditional methods, such as voltage-space vector analysis [1], voltage comparison [2], and gate voltage pattern recognition [3], offer low-latency fault identification (within one pulse-width modulation (PWM) cycle) and simple implementation. Yet, they often suffer from noise sensitivity and limited adaptability under fluctuating loads or non-ideal conditions [4]. Current-based methods such as current magnitude thresholds [5] can characterize fault dynamics effectively, but tend to lag in response time, up to 1.5 seconds and provide

Journal homepage: http://ijeecs.iaescore.com

limited localization accuracy. While traditional techniques provide low-complexity and real-time detection capabilities, they are often vulnerable in transient or noisy conditions. To improve robustness under such scenarios, researchers have explored transform-based methods. These include discrete wavelet transform (DWT) [6], short-time fourier transform (STFT) [7], [8]. These tools extract time-frequency characteristics of faults, improving detection in noisy or transient environments. Still, real-time deployment remains challenging due to computational overhead unless supported by DSPs or FPGAs.

Despite improvements from signal transforms, many of these methods still rely on manual feature extraction and domain expertise. With the rise of data-driven techniques, artificial intelligence (AI), have shown great potential in automating the detection process. An artificial neural network (ANN) approach was proposed in [9] for identifying fault signatures in inverter systems. A structured neural network system capable of detecting faults within 20 milliseconds was developed in [10]. Detection times of less than 0.1 seconds were achieved using neural networks trained on inverter switching statistics, as shown in [11].

In an effort to balance detection accuracy with practical deployment constraints, hybrid approaches combine signal processing with AI-based classification. Notable contributions include CNNs on raw currents with 99% detection in 0.64 ms and 100% localization in 1.28 ms [12], CNNs combined with STFT and fast dynamic time Warping achieving 99.4% accuracy [13], and CNNs using continuous wavelet transform (CWT) for multiclass classification achieving an accuracy of 98% in binary and 97% in multi-class classification. DWT with principal component analysis (PCA) and cuckoo search optimization (CSO)-relevance vector machine (RVM) achieved 95.67% accuracy in a relatively low response time 2.06s [14], while ANN with fast fourier transform (FFT) and DWT improved resilience to noise [15]. Comparative classifier benchmarking has shown wide variability in performance, where decision trees reached 99% accuracy but ANN models lagged behind at 37.5% [16]. Other enhancements such as multiscale CNNs incorporating temperature, voltage, and current [17], or FFT-CNN hybrids [18], have further pushed performance. These models offer flexibility but also introduce architectural complexity, requiring careful synchronization between modules and typically require large labeled datasets and significant computational resources, which may hinder deployment in real-time embedded systems.

For mission-critical applications requiring ultra-fast fault isolation, hardware-accelerated methods are a compelling alternative. Techniques such as the quasi-flying gate concept [19] and extended stray voltage capture (ESVC) [20] have achieved sub-microsecond detection speeds (< 300 ns and < 330 ns, respectively). FPGA-based monitoring solutions also demonstrate latencies under $10~\mu s$ [21]. Nonetheless, these systems tend to be rigid, expensive, and not easily scalable to new fault modes or inverter architectures.

Despite rich innovation, there is still much to be desired in order to achieves the ideal combination of speed, accuracy, robustness, scalability, and real-time deployability. Traditional methods lack adaptability, AI methods struggle with real-time constraints, and hardware approaches are rigid. This study addresses this gap by introducing a detection method that integrates: Lissajous curve-based feature extraction from output voltages; convolutional neural networks (CNNs) for classifying 18 distinct single and double switch short-circuit fault scenarios. This compact, noise-resilient, and scalable approach supports real-time deployment and enhances fault classification accuracy using geometric features of waveform behavior.

The remainder of this paper is organized as follows: section 2 describes the system modeling and fault scenario descriptions. In section 3 details the proposed fault detection and classification method. In section 4 presents and discusses the simulation results. Finally, section 5 concludes the paper and outlines future work.

2. SYSTEM MODELING

2.1. System overview

The system analyzed in this work is a conventional two-level, three-phase VSI, depicted in Figure 1. The inverter converts a constant DC input voltage V_{dc} into three-phase AC output voltages across a balanced load. It consists of six insulated gate bipolar transistors (IGBTs), labeled S_1 to S_6 , organized into three legs, each corresponding to one output phase (A, B, and C).

Each leg contains two switches operating in a complementary manner to prevent short-circuiting the DC bus. The upper and lower switches of each leg alternate according to the PWM strategy. The VSI was modeled and simulated in MATLAB/Simulink (R2023a) using the Simscape electrical toolbox. The key parameters used in the simulation are summarized in Table 1.

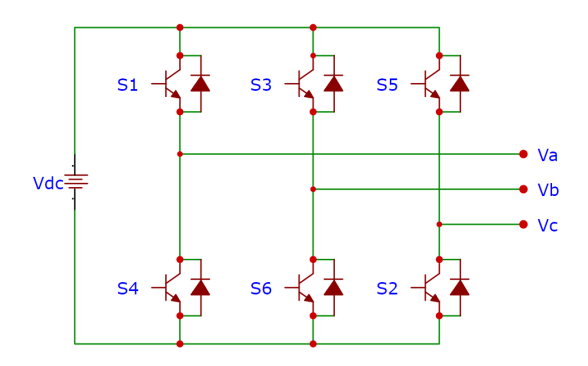


Figure 1. Three-phase two-level VSI topology under healthy conditions

Table 1. Simulation parameters

Value			
800 V			
10 kHz			
SPWM			
Balanced star-connected RL load			
$R=10~\Omega, L=5~\mathrm{mH}$			
20 kHz			
300 ms per fault case			
100 ms into simulation			

2.2. Switching control: SPWM

PWM is employed to control the timing of the IGBT switches in the VSI. In this study, sinusoidal PWM (SPWM) is chosen over other PWM techniques due to its intuitive implementation and lower computational complexity, making it well-suited for simulation environments [22]. The method operates by comparing three sinusoidal reference signals, each corresponding to one inverter phase, with a high-frequency triangular carrier wave to generate switching pulses. This results in a set of modulated gate signals that control the inverter switches and produce the desired AC output voltages.

2.3. Normal operating conditions and switching states

Under normal operation, the VSI can generate eight distinct switching states based on which of the six IGBT switches are conducting. These states yield discrete voltage levels for the three-phase outputs $(V_a, V_b, \text{ and } V_c)$. Table 2 summarizes these states with normalized phase voltages.

Table 2. Normalized phase voltage values (V_a, V_b, V_c) for different switching states under healthy conditions

State	Switches On	V_a	V_b	V_c
1	S_1, S_6, S_2	$\frac{2}{3}$	$\frac{-1}{3}$	$\frac{-1}{3}$
2	S_1, S_3, S_2	$\frac{\frac{1}{3}}{-1}$	$\frac{1}{3}$	$\frac{-2}{3}$
3	S_4, S_3, S_2	$\frac{-1}{3}$	32 3 1	$ \begin{array}{r} \hline $
4	S_4, S_3, S_5	$ \begin{array}{r} \overline{3} \\ -2 \\ \hline{3} \\ -1 \\ \hline{3} \\ \hline{1} \\ \hline{3} \end{array} $	$\frac{1}{3}$	$\frac{1}{3}$
5	S_4, S_6, S_5	$\frac{-1}{3}$	$\frac{\frac{1}{3}}{\frac{-1}{3}}$	32 31 31 3
6	S_1, S_6, S_5	<u> 1</u>	$\frac{-2}{3}$	$\frac{1}{3}$
7	S_1, S_3, S_5	ő	ő	ŏ
8	S_4, S_6, S_2	0	0	0

2.4. Fault scenarios and simulation injection approach

The inverter system is evaluated against two categories of faults: i) single-switch short-circuit faults, where one IGBT remains permanently ON, and ii) double-switch short-circuit faults, where two IGBTs are simultaneously stuck in the ON state. In total, 18 fault scenarios are simulated, comprising 6 single-switch faults and 12 double-switch faults.

ISSN: 2502-4752

Faults are introduced in the Simulink environment by overriding the PWM gate signals at a predefined instant (t = 0.1 s). The gate control signal of the affected IGBT(s) is forced to a constant high logic level ('1') for the remainder of the simulation, thereby replicating a short-circuit condition.

This modeling approach reflects industrial reality, with the two-level VSI and SPWM control representing common inverter configurations. The focus on short-circuit faults, among the most hazardous and challenging to detect, supports practical relevance. Moreover, structured fault injection combined with high-resolution sampling ensures reproducible datasets suitable for AI-based diagnostic methods, as elaborated in section 3.

3. METHOD

3.1. Simulation procedure and signal acquisition

The simulation was conducted in MATLAB/Simulink (R2023a) using the Simscape electrical environment. The modeled system is a two-level, three-phase VSI operating under SPWM at $10\,\mathrm{kHz}$, with a $800\,\mathrm{V}$ DC-link [1], [21].

Short-circuit faults were simulated by forcing selected IGBT gate signals to a constant high logic level ('1') via conditional logic blocks, emulating desaturation faults [23]. Each fault was introduced at $t=0.1\,\mathrm{s}$ and persisted for the remainder of the 300 ms run.

Phase voltages (V_a, V_b, V_c) were recorded at a sampling rate of 20 kHz. The final 100 ms of each simulation (2,000 samples) was extracted for use in the feature extraction process detailed in subsection 3.3.

To enhance generalization and simulate realistic operating conditions, two perturbations were applied: i) random variations in RL load values and ii) superimposed white gaussian noise on the DC-link ($SNR > 40 \, dB$). The resulting dataset comprises 18 fault classes (6 single-switch and 12 double-switch), with 100 simulations per class, yielding 1,800 labeled instances.

3.2. Fault behavior analysis and motivation for feature extraction

To understand how inverter faults affect voltage generation, we analyze two representative fault scenarios: a single-switch short-circuit fault in S_1 (upper IGBT of phase A) and a double-switch fault involving S_1 and S_6 (upper phase A and lower phase B) as illustrated in Figure 2. These were chosen for their high structural impact and their representativeness of other fault cases due to the inverter's symmetry.

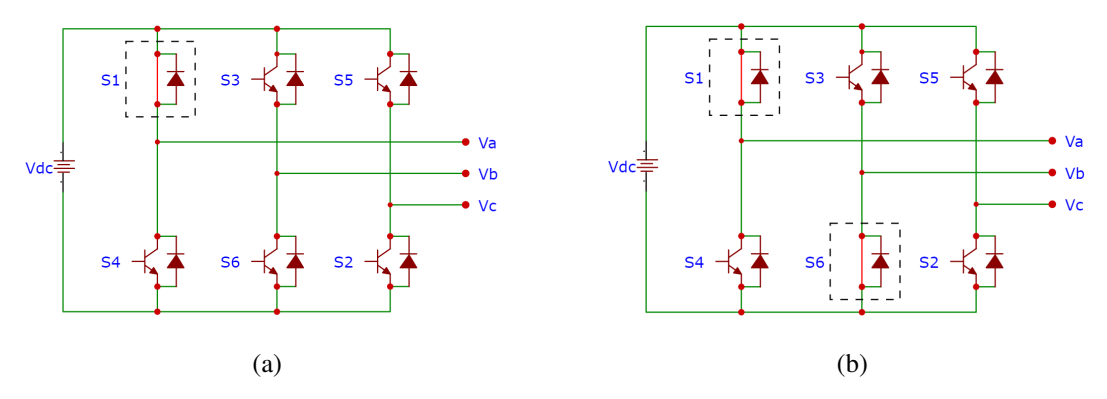


Figure 2. Inverter schematics under short-circuit conditions: (a) single-switch fault in S_1 and (b) double-switch fault in S_1 and S_6

Single-switch fault: Figure 2(a) illustrates the inverter configuration when the upper IGBT S_1 is permanently turned ON due to a short-circuit fault. Table 3 presents the corresponding output phase voltages for selected switching states. State 3, which would normally produce a distinct output, replicates the output of State 2 due to the permanent conduction of S_1 . Additionally, State 4 collapses into a zero-output condition across all phases, caused by contradictory current paths. These effects result in a loss of unique voltage states, leading to state redundancy and diminished fault distinguishability in the time-domain signals.

Double-switch fault: in the second scenario, both S_1 and S_6 remain stuck ON, as illustrated in Figure 2(b). Table 3 shows the resultant output voltages for different switching commands. States 1 through 3, which typically generate different voltage patterns, now produce identical outputs due to the fault-induced override. Similarly, States 4 and 5 also become indistinguishable, further shrinking the inverter's effective voltage-state space. This significant collapse in state resolution illustrates the limitations of conventional threshold-based or rule-based diagnostic approaches.

Conclusion: both single and double-switch short-circuit faults introduce ambiguity by forcing multiple switching states to produce the same output. This loss of resolution in the time-domain waveform space motivates the use of trajectory-based representations [24]. In this work, we exploit the interdependence of phase voltages Clarke transformation into 2D Lissajous curves, which visually reflect fault-induced distortions and are suitable for classification using CNNs.

Table 3. Phase voltage values under selected switching states for single-switch (S_1) and double-switch	l
(S_{\bullet}, S_{\circ}) faults	

		(D_1)	$, \omega_{6})$ 1	auns			
State Switches On		Single fault (S_1)			Double fault (S_1, S_6)		
State	Switches On	V_a	V_b	V_c	V_a	V_b	V_c
1	S_1, S_6, S_2	$\frac{2}{3}$	$\frac{-1}{3}$	$\frac{-1}{3}$	$\frac{2}{3}$	$\frac{-1}{3}$	$\frac{-1}{3}$
2	S_1, S_3, S_2	$\frac{1}{3}$	$\frac{1}{3}$	$\frac{-2}{3}$	$\frac{2}{3}$	$\frac{-1}{3}$	$\frac{-1}{3}$
3	S_4, S_3, S_2	$\frac{1}{3}$	$\frac{1}{3}$	$\frac{\overline{3}}{-2}$	$\frac{2}{3}$	$\frac{-1}{3}$	$\frac{-1}{3}$
4	S_4, S_3, S_5	Ŏ	Ŏ	Ŏ	$\frac{1}{3}$	$\frac{-2}{3}$	$\frac{1}{3}$
5	S_4, S_6, S_5	$\frac{1}{3}$	$\frac{-2}{3}$	$\frac{1}{3}$	$\frac{1}{3}$	$\frac{-2}{3}$	$\frac{1}{3}$
6	S_1, S_6, S_5	$\frac{1}{3}$	$\frac{-2}{3}$	$\frac{1}{3}$	$\frac{1}{3}$	$\frac{-2}{3}$	$\frac{1}{3}$

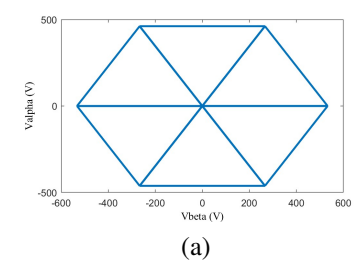
3.3. Lissajous curve-based feature extraction

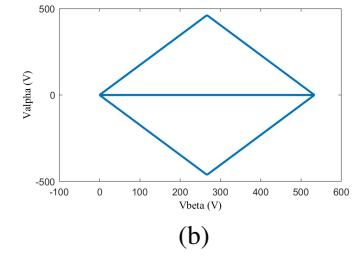
Lissajous curves offer a compact geometric representation of signal interactions and are effective for identifying inverter faults due to their sensitivity to amplitude, phase, and frequency variations [24], [25]. The three-phase voltages (V_a, V_b, V_c) are transformed into two-dimensional space-vector signals (V_α, V_β) using Clarke's transformation [26].

$$V_{\alpha} = \frac{2}{3} \left(V_a - \frac{V_b}{2} - \frac{V_c}{2} \right), \quad V_{\beta} = \frac{1}{\sqrt{3}} (V_b - V_c)$$
 (1)

Under ideal conditions, the resulting Lissajous trajectory forms a regular hexagon, with each vertex corresponding to one of the inverter's discrete switching states. When faults occur, these topological patterns become distorted, an effect that can be leveraged for classification.

Figure 3 presents representative Lissajous curves generated from the (V_{α}, V_{β}) voltage signals. In Figure 3(a), the system operates under healthy conditions, producing a well-structured, symmetric pattern. Figure 3(b) shows a single-switch fault scenario (S_1) , where distortions emerge as asymmetries. Figure 3(c) illustrates a double-switch fault $(S_1 \& S_6)$, where the pattern collapses significantly, reflecting the degraded switching behavior.





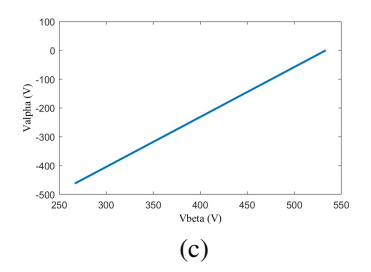


Figure 3. Lissajous curves generated from (V_a, V_b) voltage signals under different conditions; (a) healthy operation: symmetric structure, (b) single-switch fault: localized distortion, and (c) double-switch fault: severe trajectory collapse

The voltage signals are normalized to [-1, 1], and a 100 ms segment is extracted to generate grayscale Lissajous images. Each image is resized to 224×224 pixels to match the CNN input format, as detailed in subsection 3.4.

3.4. CNN architecture for fault classification

To classify Lissajous curve images into their corresponding inverter fault types, a CNN is employed. CNNs are powerful tools for image-based classification tasks due to their ability to learn spatial patterns hierarchically and automatically [13], [17].

Input: each Lissajous curve is represented as a grayscale image of size 224×224 , normalized to the range [0,1]. This image is passed as a $224 \times 224 \times 1$ tensor into the network.

Architecture: the CNN was implemented in TensorFlow 2.11 using the Keras API. The model consists of three convolutional blocks followed by dense layers, as summarized in Table 4.

rable 4. CNN architecture for classifying Lissajous curve images					
Layer	Output shape	Activation	Details		
Input layer	$224 \times 224 \times 1$	_	Grayscale image input		
Conv2D + MaxPool	$112\times112\times32$	ReLU	3×3 kernel, 2×2 pool		
Conv2D + MaxPool	$56 \times 56 \times 64$	ReLU	3×3 kernel, 2×2 pool		
Conv2D + MaxPool	$28\times28\times128$	ReLU	3×3 kernel, 2×2 pool		
Flatten	100352	-	Converts feature map to vector		
Dense + Dropout	256	ReLU	Dropout rate $= 0.5$		
Output laver	18	SoftMax	18-class classification		

Table 4. CNN architecture for classifying Lissajous curve images

The schematic architecture of the classification flow is shown in Figure 4. Each convolutional layer extracts progressively complex features from the input image, while the fully connected layers learn to map these features to the final fault class.

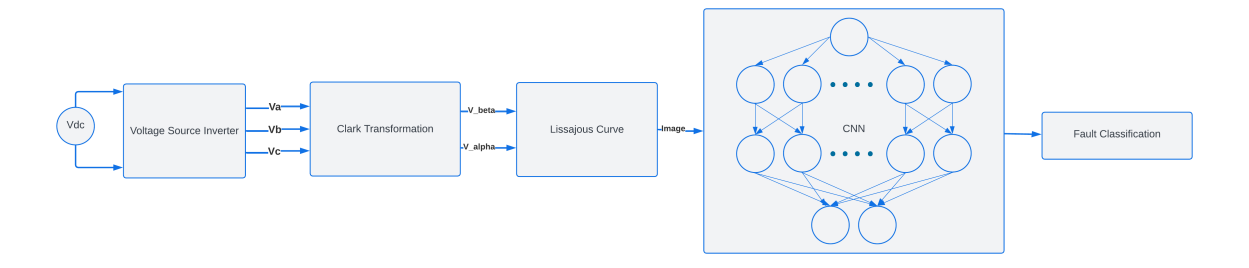


Figure 4. System architecture used for Lissajous-based fault classification

Training setup: the dataset (1,800 images across 18 classes) was divided into 80% training and 20% testing sets. Training was conducted for 50 epochs with a batch size of 32, using the Adam optimizer and categorical cross-entropy loss. No data augmentation was applied to preserve the geometric integrity of the Lissajous shapes.

Justification for CNN: CNNs are chosen over traditional machine learning methods such as support vector machines (SVM) or decision trees due to their ability to automatically extract hierarchical spatial features from image-based representations [16], [27]. This is particularly beneficial when working with Lissajous curves, as the underlying geometric distortions caused by various fault conditions are often subtle and difficult to parameterize. Furthermore, CNNs exhibit strong generalization capabilities in the presence of noise and variability in the input signals, making them well-suited for real-world inverter environments where exact waveform reproduction is not guaranteed.

Evaluation metrics: model performance was primarily assessed using overall accuracy. To evaluate class-wise effectiveness and detect potential misclassifications, precision, recall, F1-score, and a confusion matrix were computed for all fault classes.

586 □ ISSN: 2502-4752

4. RESULTS AND DISCUSSION

4.1. Visual fault signatures

Figure 5 presents representative Lissajous curves generated from (V_{α}, V_{β}) over the final 100 ms of simulation for all 18 fault types. The first row (a) displays single-switch faults, typically producing asymmetric or phase-skewed patterns. The remaining rows (b and c) correspond to double-switch faults, which lead to more severe distortions or collapsed trajectories. These fault-specific topologies are easily distinguishable and provide intuitive visual cues for classification. These spatial patterns form the core features used by the CNN, reflecting dynamic phase interactions beyond what time-domain or frequency-based methods can capture [12], [24].

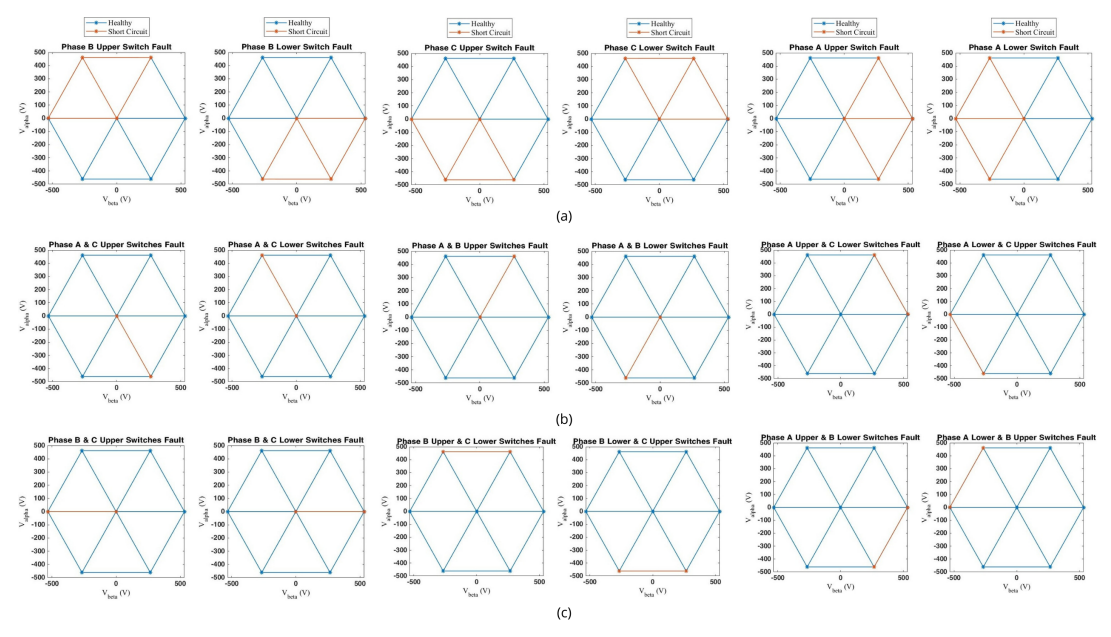


Figure 5. Lissajous curves for all fault conditions. Top row: single-switch faults (S_1-S_6) . Bottom: double-switch faults (e.g., $S_1\&S_2$, $S_3\&S_6$)

4.2. Classification performance

The CNN model was evaluated on a 20% test set (360 instances). It achieved 100% classification accuracy across all 18 fault classes, outperforming traditional and recent approaches including ANN [11] (99%), DWT + PCA + CSO-RVM [14] (95.67%), and the multiscale Kernel CNN [17] (98.3%).

Figure 6 shows the confusion matrix, with perfect diagonal alignment indicating zero misclassifications. Precision, recall, and F1-score were all equal to 1.0, confirming the model's ability to robustly learn spatial distinctions between fault-induced Lissajous signatures.

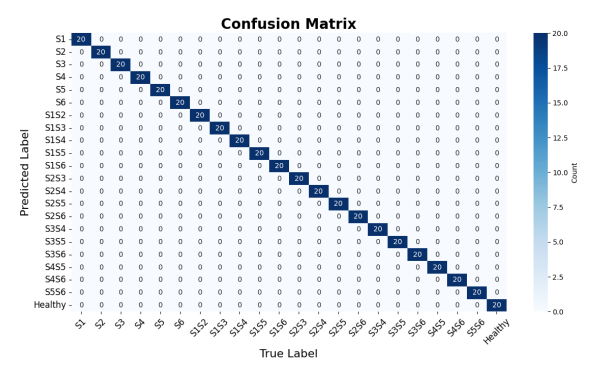


Figure 6. Confusion matrix for the 18-class CNN-based fault classifier

4.3. Class-wise interpretability

While achieving perfect accuracy, it's informative to examine feature separability. Single-switch faults (e.g., S_1 , S_3) typically yield skewed Lissajous patterns reflecting imbalance in one phase. Double-switch faults (e.g., $S_1 \& S_6$) result in collapsed or highly distorted curves due to redundant switching paths. These spatial deformations are visually distinct and stable across simulation runs.

Conventional techniques often fail in scenarios with state overlap, such as $S_1 \& S_2$ or $S_4 \& S_5$, where multiple switching commands produce identical outputs. In contrast, the CNN exploits subtle topological shifts in the Lissajous geometry to separate even these visually similar faults, addressing limitations seen in earlier works [16], [23].

4.4. Robustness to noise and variability

To test generalization, simulations were repeated under disturbances, small RL variations and white Gaussian noise (SNR $> 40 \,\mathrm{dB}$). Despite these, the CNN consistently maintained accurate predictions. This robustness stems from the geometric invariance of the Lissajous curves, whose structural features remain stable under minor waveform distortions. Importantly, the model achieves these results without data augmentation or denoising filters, highlighting the reliability of the visual representation itself. This makes the method promising for real-world inverter monitoring systems, particularly where noise and load variability are inevitable.

4.5. Summary and comparison

This study validates an end-to-end fault classification pipeline based on Lissajous curves and CNNs. The method demonstrated perfect accuracy across 18 short-circuit scenarios, requiring no manual signal engineering or hardware instrumentation. It operates solely on voltage waveforms, producing intuitive visual features that CNNs can effectively learn and generalize from.

These results confirm the initial objective outlined in section 1 developing a compact, noise-resilient, and real-time-friendly fault detection framework using Lissajous curves and CNNs. The method successfully achieves high accuracy, robustness to load and noise variation, and complete automation, demonstrating its potential for scalable deployment in industrial inverter systems.

Table 5 compares our approach with established methods. While hardware-based solutions provide faster response, they require intrusive components. In contrast, our method is entirely software-driven and non-invasive, offering high accuracy at acceptable latency.

Despite these strengths, some limitations remain: only short-circuit faults were explored, and validation was limited to simulations. Real-world deployment may require adjustments for open-switch faults, hardware noise, or sampling delays. However, the simplicity and consistency of the method suggest strong potential for integration in real-time systems.

Method	Detection time	Accuracy	Limitations
Proposed: Lissajous + CNN	100 ms	100%	Needs image generation; moderate inference time
Structured neural network [10]	20 ms	\sim 97%	Rule-based; low adaptability
Multiscale CNN [17]	60 ms	98.3%	Complex tuning; sensitive to scale
Interior-angle method [28]	1 ms	98.5%	Timing-sensitive; weak generalization
DTCWT and SVOA-based SVM [27]	50 ms	99.9%	Requires feature engineering
Manual Lissajous matching [24]	\geq 100 ms	N/A	Human-dependent; not scalable
DWT + SVM [29]	60 ms	\sim 95%	Noise-sensitive handcrafted features
Stray voltage sensor [20]	$1\mu\mathrm{s}$	N/A	Hardware required; invasive

Table 5. Comparison of VSI fault classification methods

5. CONCLUSION

This paper presents a new approach for detecting and classifying short-circuit faults in a two-level three-phase VSI using Lissajous curve representations and CNNs. By transforming time-domain voltage signals into spatially structured 2D curves, the proposed method captures fault-induced waveform distortions that are difficult to distinguish using conventional signal analysis techniques.

The system was tested on 18 fault scenarios, including both single- and double-switch short-circuit conditions, under varying noise and load perturbations. With an end-to-end image-based classification pipeline and a lightweight CNN architecture, the proposed framework achieved 100% classification accuracy without

588 □ ISSN: 2502-4752

the need for manual feature extraction or data augmentation. The results demonstrate that Lissajous curves offer a powerful and compact representation of inverter behavior, enabling robust and scalable fault diagnosis.

Future work will aim to address the issues and limitations presented in the discusion section by validating the proposed technique on hardware testbeds and exploring the use of Lissajous curves for other power electronic systems, including multilevel inverters and motor drives. Additionally, further research could investigate hybrid models that combine time-domain and image-based features for even greater diagnostic reliability.

FUNDING INFORMATION

Authors state no funding involved.

CONFLICT OF INTEREST STATEMENT

Authors state no conflict of interest.

DATA AVAILABILITY

Data availability is not applicable to this paper as no new date were created or analyzed in this study.

REFERENCES

- M. Alavi, D.Wang, and M. Luo, "Short-circuit fault diagnosis for three-phase inverters based on voltage-space patterns," IEEE Transactions on Industrial Electronics, vol. 61, no. 10, pp. 5558–5569, Oct. 2014, doi: 10.1109/TIE.2013.2297298.
- [2] S. Ouni et al., "Quick diagnosis of short circuit faults in cascaded H-bridge multilevel inverters using FPGA," Journal of Power Electronics, vol. 17, no. 1, pp. 56–66, Jan. 2017, doi: 10.6113/JPE.2017.17.1.56.
- [3] J.-B. Lee and D.-S. Hyun, "Gate voltage pattern analyze for short-circuit protection in IGBT inverters," in 2007 IEEE Power Electronics Specialists Conference, 2007, pp. 1913–1917, doi: 10.1109/PESC.2007.4342295.
- [4] C. Drif, A. Soualhi, and H. Nouri, "A technique for diagnosing short-circuit and open-circuit faults of the three-phase inverter," 2022 19th IEEE International Multi-Conference on Systems, Signals and Devices, SSD 2022, pp. 92–96, 2022, doi: 10.1109/SSD54932.2022.9955675.
- [5] B. J. Hyon, D. Y. Hwang, P. Jang, Y.-S. Noh, and J.-H. Kim, "Offline fault diagnosis for 2-level inverter: short-circuit and open-circuit detection," *Electronics*, vol. 13, no. 9, p. 1672, Apr. 2024, doi: 10.3390/electronics13091672.
- [6] A. M. Khalkho, S. Das, and A. K. Chattopadhyay, "Phase disposition PWM five-level inverter short switch diagnosis using DWT and Ann," in *Michael Faraday IET International Summit 2015*, 2015, vol. 2015, no. CP683, p. 70, doi: 10.1049/cp.2015.1666.
- [7] M. Manap, S. Nikolovski, A. Skamyin, R. Karim, T. Sutikno, and M. H. Jopri, "An analysis of voltage source inverter switches fault classification using short time fourier transform," *International Journal of Power Electronics and Drive Systems (IJPEDS)*, vol. 12, no. 4, pp. 2209–2220, 2021, doi: 10.11591/ijpeds.v12.i4.pp2209-2220.
- [8] Y. M. Yeap, N. Geddada, K. Satpathi, and A. Ukil, "Time- and frequency-domain fault detection in a VSC-interfaced experimental DC test system," *IEEE Transactions on Industrial Informatics*, vol. 14, no. 10, pp. 4353–4364, Oct. 2018, doi: 10.1109/TII.2018.2796068.
- [9] M. Abid, S. S. Laribi, Z. S. Al-asgar, and M. Larbi, "Artificial neural network approach assessment of short-circuit fault detection in a three phase inverter," in 2021 International Congress of Advanced Technology and Engineering (ICOTEN), Jul. 2021, pp. 1–5, doi: 10.1109/ICOTEN52080.2021.9493498.
- [10] M. Abul Masrur, Z. Chen, and Y. Murphey, "Intelligent diagnosis of open and short circuit faults in electric drive inverters for real-time applications," *IET Power Electronics*, vol. 3, no. 2, pp. 279–291, Mar. 2010, doi: 10.1049/iet-pel.2008.0362.
- [11] M. U. Oner, İ. Şahin, and O. Keysan, "Neural networks detect inter-turn short circuit faults using inverter switching statistics for a closed-loop controlled motor drive," *IEEE Transactions on Energy Conversion*, vol. 38, no. 4, pp. 2387–2395, Dec. 2023, doi: 10.1109/TEC.2023.3274052.
- [12] D. Łuczak, S. Brock, and K. Siembab, "Fault detection and localisation of a three-phase inverter with permanent magnet synchronous motor load using a convolutional neural network," Actuators, vol. 12, no. 3, 2023, doi: 10.3390/act12030125.
- [13] N.-C. Yang and J.-M. Yang, "Fault classification in distribution systems using deep learning with data preprocessing methods based on fast dynamic time warping and short-time fourier transform," *IEEE Access*, vol. 11, pp. 63612–63622, 2023, doi: 10.1109/AC-CESS.2023.3288852.
- [14] V. Gomathy and S. Selvaperumal, "Fault detection and classification with optimization techniques for a three-phase single-inverter circuit," *Journal of Power Electronics*, vol. 16, no. 3, pp. 1097–1109, May 2016, doi: 10.6113/JPE.2016.16.3.1097.
- [15] A. Athimoolam and K. Balasubramanian, "Fault recognition of multilevel inverter using artificial neural network approach," *Intelligent Automation & Soft Computing*, vol. 36, no. 2, pp. 1331–1347, 2023, doi: 10.32604/iasc.2023.033465.
- [16] K. A. Mahafzah, M. A. Obeidat, A. M. Mansour, A. Q. Al-Shetwi, and T. S. Ustun, "Artificial-intelligence-based open-circuit fault diagnosis in VSI-Fed PMSMs and a novel fault recovery method," Sustainability, vol. 14, no. 24, p. 16504, Dec. 2022, doi: 10.3390/su142416504.
- [17] A. Sivapriya, N. Kalaiarasi, R. Verma, B. Chokkalingam, and J. L. Munda, "Fault diagnosis of cascaded multilevel inverter using multiscale kernel convolutional neural network," *IEEE Access*, vol. 11, pp. 79513–79530, 2023, doi: 10.1109/AC-CESS.2023.3299852.

- ISSN: 2502-4752
- [18] Y. Tamissa, F. Charif, F. Kadri, and A. Benchabane, "Pattern recognition and diagnosis of short and open circuit faults inverter in induction motor drive using neural networks," *Engineering Review*, vol. 42, no. 3, 2022, doi: 10.30765/ER.1949.
- [19] M. Picot-Digoix, F. Richardeau, J.-M. Blaquière, S. Vinnac, S. Azzopardi, and T.-L. Le, "Quasi-flying gate concept used for short-circuit detection on SiC power MOSFETs based on a dual-port gate driver," *IEEE Transactions on Power Electronics*, vol. 38, no. 6, pp. 6934–6938, Jun. 2023, doi: 10.1109/TPEL.2023.3258640.
- [20] M. Al Sakka, F. Hosseinabadi, T. Geury, M. El Baghdadi, M. Al Sakka, and O. Hegazy, "Extension of the stray voltage capture short-circuit detection method to a 6-phase fault-tolerant dual-motor drive," *IEEE Open Journal of Power Electronics*, vol. 5, pp. 135–144, 2024, doi: 10.1109/OJPEL.2024.3352117.
- [21] S. Karimi, P. Poure, and S. Saadate, "Fast power switch failure detection for fault tolerant voltage source inverters using FPGA," *IET Power Electronics*, vol. 2, no. 4, pp. 346–354, Jul. 2009, doi: 10.1049/iet-pel.2008.0075.
- [22] N. Singh and I. Khan, "Scheme and Simulation of SVPWM and SPWM based on two level VSI for Grid connected PV System," in 2020 International Conference on Advances in Computing, Communication & Materials (ICACCM), Aug. 2020, pp. 1–7, doi: 10.1109/ICACCM50413.2020.9212927.
- [23] M. A. Awadallah, M. M. Morcos, S. Gopalakrishnan, and T. W. Nehl, "Detection of stator short circuits in VSI-fed brush-less DC motors using wavelet transform," *IEEE Transactions on Energy Conversion*, vol. 21, no. 1, pp. 1–8, Mar. 2006, doi: 10.1109/TEC.2005.847964.
- [24] S. Kharoubi and L. El Menzhi, "Wind turbine doubly-fed induction generator defects diagnosis using rotor currents lissajous curves," *International Journal of Power Electronics and Drive Systems (IJPEDS)*, vol. 11, no. 4, p. 2083, Dec. 2020, doi: 10.11591/ijpeds.v11.i4.pp2083-2090.
- [25] A. Gallozzi and R. M. Strollo, "Between mechanics and harmony: the drawing of lissajous curves," Foundations of Science, vol. 29, no. 1, pp. 205–224, Mar. 2024, doi: 10.1007/s10699-023-09906-z.
- [26] M. Ravi and R. C. Kumaran, "Modelling and simulation of transformer less dynamic voltage restorer for power quality improvement using combined Clark's and Park's transformation technique," Advances in Intelligent Systems and Computing, vol. 467, pp. 513–521, 2017, doi: 10.1007/978-981-10-1645-5_43.
- [27] S. R. Mestha and N. Prabhu, "Support vector machine based fault detection in inverter-fed electric vehicle," Energy Storage, vol. 6, no. 1, Feb. 2024, doi: 10.1002/est2.576.
- [28] M. Pourmirasghariyan, S. F.Zarei, M. Hamzeh, and F. Blaabjerg, "An interior-angle analysis of power for fault detection in VSC-based HVDC-grids," *International Journal of Electrical Power & Energy Systems*, vol. 159, p. 110058, Aug. 2024, doi: 10.1016/j.ijepes.2024.110058.
- [29] B. A. Vinayak, K. A. Anand, and G. Jagadanand, "Wavelet-based real-time stator fault detection of inverter-fed induction motor," IET Electric Power Applications, vol. 14, no. 1, pp. 82–90, Jan. 2020, doi: 10.1049/iet-epa.2019.0273.

BIOGRAPHIES OF AUTHORS



Sai Aioub © 🖾 🗷 was born in Morocco on february 1997. In 2021, he received an Enginering degree in Electronic Systems and Control from the National School of Applied Sciences, Abdelmalek Essaadi University of Morocco in Tangier. He, then, recieved a master degree in control, signal, and image processing in 2022 from the University of Paris-Saclay in Paris, France. He is a Ph.D. student in Electricotechnical engineering at National School of Applied Sciences in Tangier since novembre 2022. He is interested in electrical machines and electrical devices modeling, control and on-line diagnosis defects. He can be contacted at email: aioub.sai@etu.uae.ac.ma.





El Menzhi Lamiaâ si sa professor in Abdelamalek Essaadi University in Morocco since 2010. On 2002, She got her High Deepened Studies Diploma in electrical engineering from the High National School of Electricity and Mechanics ENSEM in Hassan 2 University in Casablanca. From 2002 until 2004, she was a research student in one of the universities in japan. On 2009, she obtained her Doctor degree, then her Habilitation as a professor researcher on 2016 from Hassan 2 University in Casablanca (ESEM). She is interested in electrical machines control and on-line diagnosis either used as a motor or a generator in wind turbines. Lamiaa El Menzhi is a member and advisor of the Moroccan Center of Polytechnical Research and Innovation since 2015. She can be contacted at email: lamdockit@yahoo.com.